

MULTIPLE SCATTERING IN CLUMPY MEDIA. II. GALACTIC ENVIRONMENTS

ADOLF N. WITT

Ritter Astrophysical Research Center, The University of Toledo
Toledo, OH 43606; awitt@dusty.astro.utoledo.edu

AND

KARL D. GORDON¹

Department of Physics & Astronomy, Louisiana State University
Baton Rouge, LA 70803; gordon@dirty.phys.lsu.edu

Draft version September 8, 2018

ABSTRACT

We present and discuss the results of new multiple-scattering radiative transfer calculations for three representative types of galactic environments, filled with either homogeneous or two-phase clumpy dust distributions. Extinction and scattering properties for two types of interstellar dust, similar to those found in the average diffuse medium of the Milky Way Galaxy (MW) and the Bar of the Small Magellanic Cloud (SMC), are considered. The wavelength coverage extends from 1000 Å to 30,000 Å, with particular emphasis on the rest-frame UV. This makes these models especially applicable to starburst galaxies and Lyman-break galaxy samples. The examination of the models concentrates on the study of UV/visual/near-IR reddening effects, the wavelength dependence of attenuation, and on the changes that arise from the transition from homogeneous to clumpy dust distributions in different star/dust geometries. Embedded dust, especially when clumpy, leads to saturation at fairly low reddening values with correspondingly gray attenuation functions. This makes the assessment of the attenuation of the far-UV flux from starburst galaxies difficult, if only UV/visual/near-IR data are available. Existing data for UV-selected starburst galaxies indicate a range of UV attenuation factors of 0–150. Our models reproduce the “Calzetti Attenuation Law”, provided one adopts SMC-type dust and a clumpy shell-type dust distribution surrounding the starbursts. The average far-UV attenuation factor for the Calzetti sample is found to be 7.4. The only relatively reliable measure for the UV attenuation factor for single galaxies was found in the ratio of the integrated far-IR flux to the far-UV flux, measured near 1600 Å, requiring the measurement of the entire spectral energy distribution of galaxies.

Subject headings: dust extinction – radiation transfer

1. INTRODUCTION

The presence of dust in galaxies has a profound impact on observable characteristics such as their apparent UV/optical/near-IR luminosity, their spectral energy distribution, their recognizable level of star-formation activity, and their morphology. In addition, dust directly affects and often controls the physical conditions within the interstellar medium of galaxies and plays a major role in interstellar chemistry by providing the sites for the formation of interstellar molecular hydrogen and by regulating the interstellar radiation field. Quantitative estimates of the dust mass responsible for the observed effects are needed in order to yield gas-to-dust ratios in galaxies of different types, essential if we are to understand the chemical evolution of galaxies over cosmological time scales.

Radiative transfer simulations often provide the most direct way to arrive at a quantitative assessment of the ways that lead to observed dust effects, provided such simulations are sufficiently realistic to apply to actual physical systems. All such simulations involve approximations. Historically, these have ranged from the adoption of absorbing screen geometries (Holmberg 1958, 1975) in analogy to the study of extinction of starlight in our Galaxy, to the consideration of various geometries with embedded dust, including the effects of multiple scattering (Witt,

Thronson, & Capuano 1992, hereafter WTC; Bruzual et al. 1988). According to WTC, a galaxy may be looked upon as consisting of environments which are characterized by certain geometrical relations between the attenuating dust and the illuminating stars. For example, starburst regions may be approximated by regions occupied by luminous stars, surrounded on the outside by the remnants of molecular clouds from which the stars originated. Quiescent parts of dusty disk galaxies may resemble systems in which stars and dust are fairly uniformly mixed, or, if one considers the same case at longer wavelengths where the dominant sources might be K-giants, a case where the scale height of sources is much larger than the scale height of the dust which is concentrated toward the center or central plane. As shown by WTC, equal amounts of dust in these different configurations produce very different reddening and attenuation effects. For the analysis of effects resulting from changes in the inclination of disk galaxies, disk models with embedded dust have been developed, either in plane-parallel or doubly exponential geometry (e.g. Bruzual et al. 1988; Byun et al. 1994; di Bartolomeo et al. 1996; Corradi et al. 1996). All of the models mentioned so far consistently illustrate the fact that a certain quantity of embedded dust produces much smaller attenuation effects than a foreground screen made from the same amount of

¹Present address: Steward Observatory, University of Arizona, Tucson, AZ 85721

dust, and that the inclusion of multiple scattering reduces these effects even further by returning the scattered radiation to the optical radiation field, albeit with an altered spectral and directional distribution.

An approximation in common among all the models mentioned above is the homogeneous nature of their assumed dust distributions, which are either constant or of a monotonically varying continuous variety. In the first paper in the present series (Witt & Gordon 1996, hereafter WG96), we conducted an extensive exploration of the effects of clumpiness on the transport of radiation through a spherical system containing scattering dust and a single central source. This study, together with the results of earlier work on transfer through clumpy media (e.g. Natta & Panagia 1984; Boissé 1990; Hobson & Scheuer 1993) clearly revealed that the clumpy multi-phase structure of the interstellar medium (ISM) leads to a significant reduction in the opacity produced by a given distribution and mass of interstellar dust. In addition, WG96 showed that the relationship between the effective optical depth of a clumpy distribution and that of an equivalent homogeneous distribution is non-linear; this leads to an effective attenuation as a function of wavelength that differs from the opacity law intrinsic to the dust in the system. These conclusions have been further amplified in a recent investigation of the radiative transfer in the clumpy environment of young stellar objects by Wolf, Fischer, & Pfau (1998) and general investigation of clumpy radiative transfer by Városi & Dwek (1999). Since clumpiness is a reality of the ISM wherever it can be observed with sufficient spatial resolution, we are introducing it into the transfer of radiation in such galactic environments as investigated in WTC now. A preliminary version of some aspects of this work appeared in Gordon, Calzetti, & Witt (1997).

In addition to adding models with a clumpy two-phase structure, we have improved several other aspects of the original WTC study. Our knowledge of dust scattering properties in the UV has greatly improved since 1992, and with some confidence we are now modeling the transfer for 15 (out of a total of 25) bandpasses in the wavelength range from 1000 Å to 3000 Å, compared to two in WTC. This improved UV coverage makes the current models particularly well suited for the analysis of starburst galaxies, both nearby and at high redshift, since these systems emit much of their stellar energy at UV wavelengths. Furthermore, most previous multi-wavelength radiative transfer studies have assumed opacity functions and scattering properties representative of average Milky Way (MW) dust. Even within the MW dust characteristics vary from one environment to another (e.g. Fitzpatrick 1999) and already in the local group of galaxies there exists a considerable variety of opacity laws (Bianchi et al. 1996; Gordon & Clayton 1998; Misselt, Clayton, & Gordon 1999). In starburst galaxies, in particular, it has been shown (Gordon et al. 1997) that the opacity function intrinsic to the dust present there is much more similar to dust found typically in the Bar of the Small Magellanic Cloud (SMC). We therefore model all our galactic environments with both the average MW and SMC bar dust. Other radiative transfer studies which have included both MW and SMC bar type dust are those detailed by Gordon et al. (1997), Takagi, Arimoto, & Vansevicius (1999), and Ferrara et al. (1999). The models

presented in the present paper are particularly well suited to analyze the reddening effects and the corresponding UV attenuation in Lyman-break galaxies and galaxies seen in the Hubble deep fields (Dickinson 1997; Meurer et al. 1997; Meurer, Heckman, & Calzetti 1999; Sawicki et al. 1997; Sawicki & Yee 1998, Steidel et al. 1999). They are equally well usable for studying opacity effects in nearby dusty galaxies (e.g. Berlind et al. 1997; Gordon et al. 1997; Kuchinski et al. 1998; Smith, Herter, & Haynes 1998). The principal results from the current work are an extensive set of tables, accessible in the on-line version of this issue of *The Astrophysical Journal* or available by contacting the authors. We will present the details of the models in the following Section 2; selected results will be summarized in graphical form in Section 3; we will discuss the implications of these results for currently ongoing galaxy studies in Section 4, to be followed by a summary in Section 5.

2. MODEL

In order to model the dust radiative transfer in complex systems such as galaxies, we use a radiative transfer model (named DIRTY) based on Monte Carlo techniques (Witt 1977). Use of such a model allows for arbitrary distributions of both the emitting sources (stars) and absorbing and scattering material (dust). The full description of DIRTY can be found in Gordon et al. (1999b). The inputs to DIRTY are the stellar distribution, the dust distribution, and the dust grain properties. With Monte Carlo techniques, individual photons are emitted isotropically from stars according to the stellar distribution and followed through a dust distribution. Each photon's interaction with the dust is parameterized by the dust optical depth (τ), albedo, and scattering phase function. The optical depth determines where the photon interacts, the albedo gives the probability the photon is scattered from a dust grain, and the scattering phase function gives the angle at which the photon scatters.

2.1. Dust and Stellar Distributions

As was done in WTC, we have chosen to model spherical galactic environments instead of entire galaxies. A galactic environment describes the distribution of the stars and gas. In this paper we concentrate on three galactic environments: CLOUDY, DUSTY, and SHELL. These three geometries span the range of star/dust distributions and are pictorially represented in Figure 1. The CLOUDY geometry has dust extending to 0.69 of the system radius and stars extending to the system radius. The DUSTY geometry has both dust and stars extending to the system radius. This geometry represents a uniform mixture of stars and dust. The SHELL geometry has stars extending to 0.3 of the system radius and dust extending from 0.3 to 1 of the system radius. This geometry was named nuclei in WTC.

These three geometries characterize the *global* star and dust distribution. The *local* distribution of the dust can be either homogeneous or clumpy. For this paper, we define the clumpy distribution (using the definitions of WG96) to have a filling factor (ff) of 0.15, a low-density to high-density ratio (k_2/k_1) of 0.01, and a system size characterized by a cube divided into 30^3 cubical bins ($N = 30$). A forthcoming third paper in this series will present the radiative transfer through doubly exponential disk/bulge

galaxies with clumpy ISM.

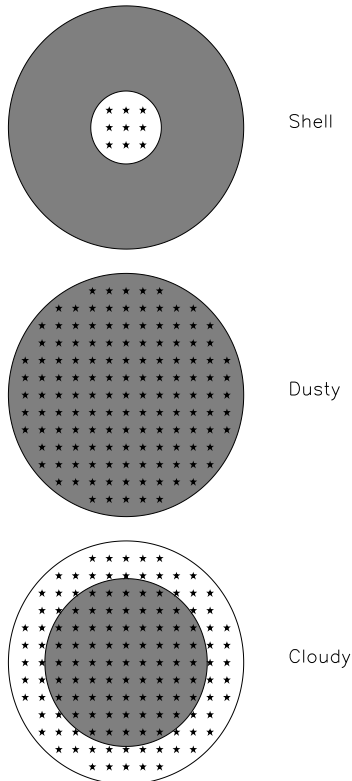


FIG. 1.— Pictorial representation of the three geometries used in this paper (SHELL, DUSTY, and CLOUDY). The star symbols trace the stellar distribution and the grey solid regions give the dust distribution.

2.2. Dust Grain Characteristics

We have chosen to compute models using both Milky Way (MW) and Small Magellanic Cloud (SMC) dust. By using these two different types of dust, we are spanning the range of *known* dust extinction curves. For Monte Carlo radiative transfer, we need to know the dependence of the dust’s optical depth (τ), albedo (a), and scattering phase function on wavelength. In this work, we used the Henyey & Greenstein (1941) phase function which is parameterized by the phase function weighted average of the cosine of the scattering angle ($g = \langle \cos\theta \rangle$).

For the MW, we used dust which is associated with the diffuse interstellar medium and has $R_V = A_V/E(B-V) = 3.1$. The wavelength dependence of τ was determined from the parameterization of Milky Way extinction curves by Cardelli, Clayton, & Mathis (1991, hereafter CCM). The a and g values were determined by comparing empirical determinations of these numbers to a dust grain model which reproduces the $R_V = 3.1$ extinction curve (Kim, Martin, & Hendry 1994). Figure 2a shows the empirical determinations, dust grain model values, and the numbers adopted in this paper. In determining the albedo values to use for this paper, we visually averaged the empirical determinations and then shifted the average to agree with the dust grain model values. The shift was done because

most of the empirical determinations were done for reflection nebulae which usually have higher values of R_V than 3.1. The dust grain model predicts decreasing albedo’s for decreasing R_V ’s. This is also consistent with recent work on the ultraviolet diffuse galactic light (Witt, Friedmann, & Sasseen 1997). When we averaged the albedo values, we also made sure that $Q_{\text{sca}} (= aQ_{\text{ext}})$ was smooth across the 2175 Å bump as it is an absorption feature (Calzetti et al. 1995). Figure 3a plots Q_{ext} , Q_{sca} , and Q_{abs} for the MW albedo values used in this paper. The g values shown in Fig. 2b were taken as averages of the empirical determinations, as the g values from the ultraviolet diffuse galactic light work are not significantly different from those of work on reflection nebulae. Also, the dust grain model still has problems in that it predicts the 2175 Å bump as partly a scattering feature, contrary to observational evidence. The τ , a , and g values adopted for MW dust in this paper are given in Table 1.

For the SMC, we used dust which is associated with the star forming Bar of the SMC (Gordon & Clayton 1998). This dust produces extinction curves which are quite different from dust extinction curves in the MW (CCM) or the Large Magellanic Cloud (Misselt, Clayton, & Gordon 1999). It lacks a 2175 Å bump and is roughly linear with λ^{-1} . This type of dust seems to be associated with intense star forming regions (Gordon et al. 1997; Gordon & Clayton 1998; Misselt, Clayton, & Gordon 1999). The τ values were taken from an average of the three known extinction curves in the SMC Bar (Gordon & Clayton 1998). There is no empirical work on the a and g values in the SMC. As there are also still problems with dust grain models reproducing the MW a and g values, we have chosen to start with the MW a values and then modify them to reflect the lack of a 2175 Å bump. This time, we required that the Q_{sca} and Q_{abs} values did not show any features across the 2175 Å region. Figure 3b displays Q_{ext} , Q_{sca} , and Q_{abs} for the SMC albedo values used in this paper. The τ , a , and g values adopted for SMC dust in this paper are given in Table 1.

3. RESULTS

3.1. Structure of the Data Tables

The results of our radiative transfer calculations are contained in Tables 2, 3, and 4, accessible in full in the online edition of this issue or available directly from the authors. Table 2 contains the data for the DUSTY galactic environment, Table 3 those for the SHELL galactic environment, and Table 4 those for the CLOUDY environment. Only the beginning of Table 2 is shown in this paper in order to illustrate the type of data available in the full set of tables. Each model is identified by its geometry (DUSTY, SHELL, CLOUDY), the intrinsic opacity function (MW, SMC), the radial extinction optical depth from the center to the edge of the dust environment at V ($\tau_V = 0.25, 0.5, \dots, 50$), assuming a constant density homogeneous distribution, and the type of structure (homogeneous, clumpy) in the dust region. Each individual model contains calculations for 25 wavelengths, ranging from 1000 Å to 30000 Å, shown in column 1. Column 2 identifies the optical depths for extinction at each wavelength, derived from the applicable intrinsic opacity function. Columns 3, 4, 5, and 6 list, respectively, the attenuation optical depth (τ_{att}), the

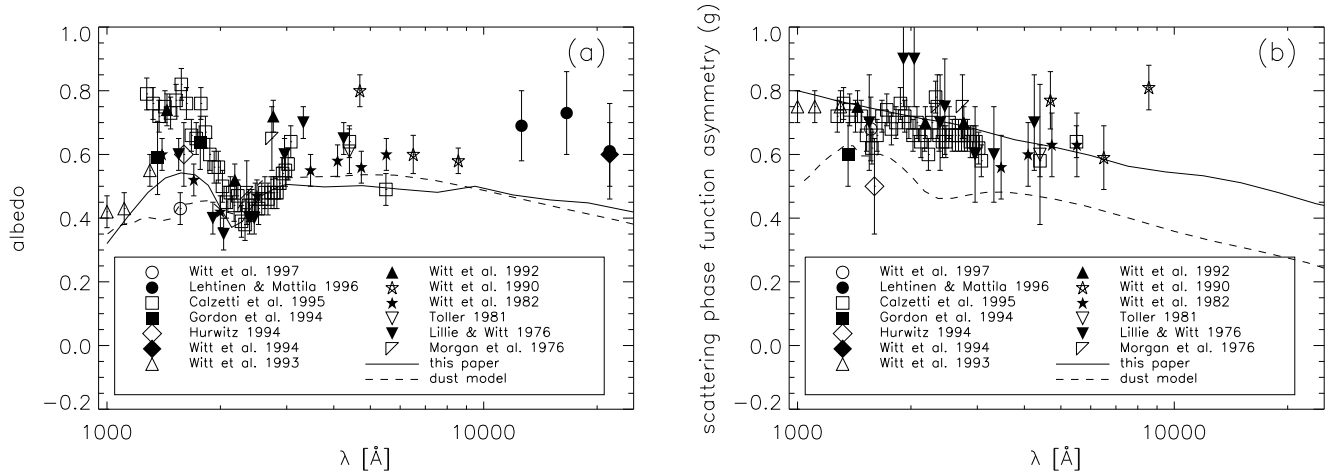


FIG. 2.— The albedo (a) and scattering phase function asymmetry (g) values are plotted as a function of wavelength in (a) and (b), respectively. This plot includes values from empirical determinations from the literature, a dust grain model (Kim et al. 1994), and numbers adopted for this paper.

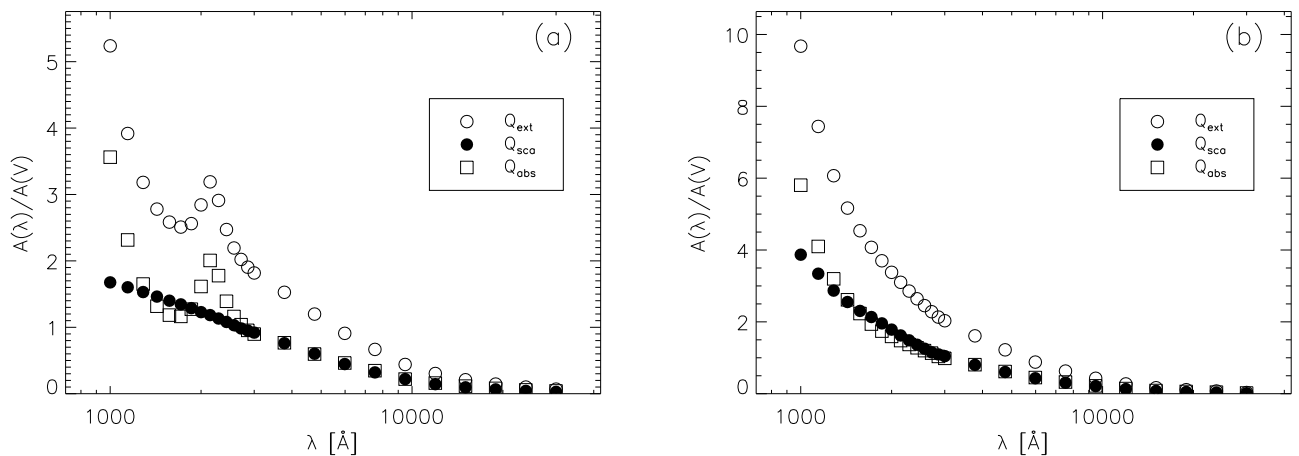


FIG. 3.— The various Q values for the MW and SMC are plotted in (a) and (b), respectively.

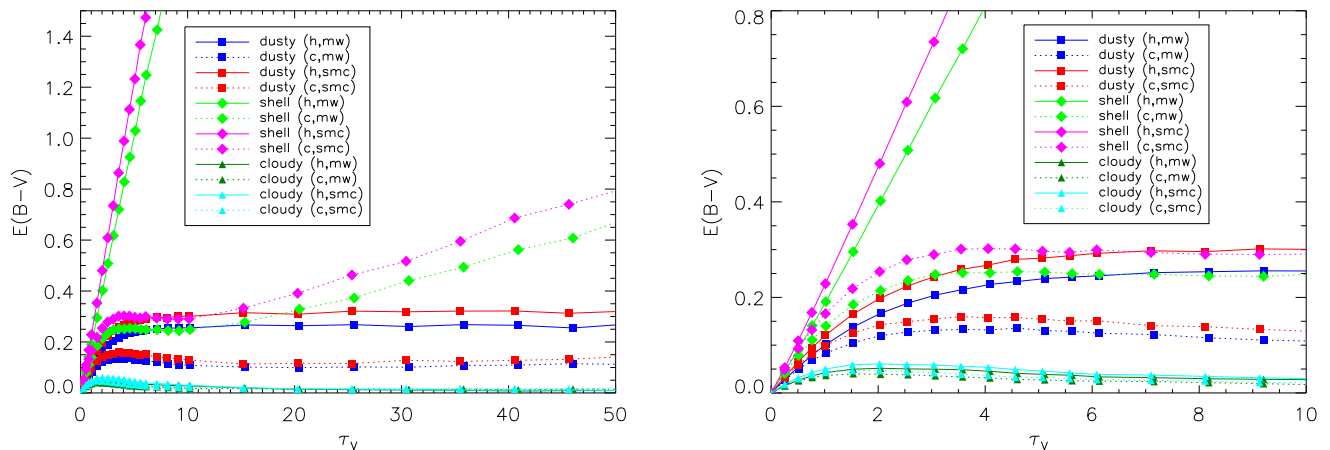


FIG. 4.— The traditional reddening signature of dust $[E(B-V)]$ is plotted versus the input τ_V (proportional to dust mass) in (a). In (b), a blowup of this plot is shown to illustrate the behavior of $E(B-V)$ for τ_V values < 10 .

TABLE 1
DUST PHYSICAL PROPERTIES

λ [Å]	τ/τ_V	MW		τ/τ_V	SMC	
		a	g		a	g
1000.0	5.238	0.320	0.800	9.675	0.400	0.800
1142.9	3.918	0.409	0.783	7.440	0.449	0.783
1285.7	3.182	0.481	0.767	6.068	0.473	0.767
1428.6	2.780	0.526	0.756	5.167	0.494	0.756
1571.4	2.584	0.542	0.745	4.536	0.508	0.745
1714.3	2.509	0.536	0.736	4.074	0.524	0.736
1857.1	2.561	0.503	0.727	3.700	0.529	0.727
2000.0	2.843	0.432	0.720	3.379	0.528	0.720
2142.9	3.190	0.371	0.712	3.101	0.523	0.712
2285.7	2.910	0.389	0.707	2.857	0.520	0.707
2428.6	2.472	0.437	0.702	2.642	0.516	0.702
2571.4	2.194	0.470	0.697	2.452	0.511	0.697
2714.3	2.022	0.486	0.691	2.282	0.505	0.691
2857.1	1.905	0.499	0.685	2.133	0.513	0.685
3000.0	1.818	0.506	0.678	2.031	0.515	0.678
3776.8	1.527	0.498	0.646	1.610	0.498	0.646
4754.7	1.199	0.502	0.624	1.221	0.494	0.624
5985.8	0.909	0.491	0.597	0.880	0.489	0.597
7535.8	0.667	0.481	0.563	0.630	0.484	0.563
9487.0	0.440	0.500	0.545	0.430	0.493	0.545
11943.5	0.304	0.473	0.533	0.272	0.475	0.533
15036.0	0.210	0.457	0.511	0.166	0.465	0.511
18929.2	0.145	0.448	0.480	0.111	0.439	0.480
23830.6	0.100	0.424	0.445	0.075	0.417	0.445
30001.0	0.069	0.400	0.420	0.033	0.400	0.420

scattered flux fraction, the direct attenuated stellar flux fraction, and the total escaping flux fraction, containing both attenuated stellar as well as scattered radiation, for the homogeneous case. Columns 7 to 10 repeat this information for the equivalent clumpy case. All fluxes are referred to unity at each wavelength, with unit flux corresponding to no attenuation, and in cases with clumpy dust distributions, they are averages over all directions.

For a given geometry, the value of the V-band optical depth may be regarded as a measure of the dust mass present in that geometry. The attenuation optical depth (column 3 and 7) is defined as

$$\tau_{\text{att}} = -\ln(f(\text{esc})) \quad (1)$$

and thus measures the absorption occurring in the system. This is a rather useful measurement since in galactic environments viewed from afar both the attenuated stellar flux as well as the scattered light are combined in the escaping total flux observed. Note that this definition of the attenuation optical depth differs from that of the effective optical depth (τ_{eff}) defined in WG96, which refers to the attenuated, non-scattered stellar flux only. The τ_{att} values are always smaller than the radial optical depth listed in column 2, because the dust albedo is always non-zero and the stars are distributed throughout extended volumes. Also, the attenuation optical depth for the clumpy cases never exceeds that of the corresponding homogeneous cases (WG96). It needs to be reemphasized that the clumpy case treated here is for one specific set of clumpiness parameters, namely a filling factor $\text{ff} = 0.15$, an interclump medium to clump density ratio $k_2/k_1 = 0.01$, and a system size divided into 30^3 cubical bins. The variations of transfer characteristics expected when any of these parameters are changed within reasonable ranges were explored in WG96, and they are briefly discussed in Section 3.5.

3.2. Reddening Effects

Reddening of a spectral energy distribution compared to that expected from spectroscopic indicators is usually taken as the first sign of the presence of dust in a galactic system. Color-color diagrams derived from multi-color photometry of galaxies frequently exhibit reddening *arrows* which purport to show the direction in which data points move in the color-color plane in response to the presence of a given column density of dust. Implicit in such displays is the assumption that the reddening is proportional to the dust column. It was shown by WTC that the relationships between reddenings and dust columns is usually quite non-linear and highly dependent upon details of the geometry and the scattering properties of the dust. Here we show the additional effects due to the presence of a clumpy structure in the attenuating medium.

In Fig. 4a we show the traditional reddening parameter $E(B - V)$ as a function of the homogeneous radial optical depth τ_V ; in Fig. 4b the congested region near the origin of Fig. 4a is enlarged. Several interesting points can be made. The most dramatic effect arising from the transition from a homogeneous structure to a two-phase clumpy structure occurs in the SHELL geometry. The homogeneous SHELL is similar to a spherical homogeneous screen, except that flux is scattered back into the beam in the SHELL geometry. As expected for a screen, the predicted reddening for

the homogeneous SHELL geometry increases linearly with increasing dust column density. The scaling factor is less than that for a screen due to the blue color of scattered radiation included in the measurement. Consequently, the ratios $E(B - V)/\tau_V$ for the homogeneous SHELL models are 0.20 for the MW case, 0.24 for the SMC case. This should be compared to the standard ratio of 0.35 for average Galactic extinction. The transition to a two-phase clumpy dust structure in the shell leads to a reddening function which quickly becomes non-linear and saturates near $E(B - V) \sim 0.25$ for MW dust, near $E(B - V) \sim 0.30$ for SMC dust. This initial saturation is caused by the fact that individual clumps become optically thick while the low-density interclump medium initially contributes little to the reddening. At $\tau_V > 10$, the clumpy SHELL geometry exhibits a gradual increase in the reddening again, now solely due to the growing attenuation by the interclump medium. Note the interesting parallel to the behavior of a curve-of-growth in astronomical spectroscopy, where the increase of absorption in the core of a line is followed by saturation and subsequent further growth due to absorption in the damping wings of the line.

The DUSTY geometry exhibits a permanent saturation at larger optical depths both in the clumpy and in the homogeneous states, as was shown already by WTC. The transition to a clumpy structure makes the saturation occur at roughly half the amount of reddening in $E(B - V)$ than was found in the homogeneous case. The saturation in the homogeneous case is a result of the fact that radiation emerges primarily from the outermost regions within optical depths one to two, regardless of how much dust is present further inside the system. This is fundamentally unchanged by adopting a clumpy structure, except that light now escapes preferentially through low-optical depth lines-of-sight between clumps, resulting in an overall lower amount of reddening.

The level of $E(B - V)$ at which realistic dusty structures saturate is highly significant. It has been noted with great emphasis by Dickinson (1997), Sawicki and Yee (1998), and Steidel et al. (1999), among others, that the $E(B - V)$ color excesses of Lyman-break galaxies crowd around values of $E(B - V) \sim 0.2$, with hardly any exhibiting color excesses greater than 0.35. This result is fully consistent with our model results. All models except the homogeneous SHELL models saturate at reddening values $E(B - V)$ less than 0.3, a value which is breached by the clumpy SHELL models only for $\tau_V > 15$. This suggests that the highly idealized homogeneous SHELL model, which is basically the historical screen model with scattering, does not apply to these Lyman-break galaxies, as was argued forcefully by WTC already. However, the result also means that the actual dust column densities and the resulting attenuations are quite unconstrained by these color excess measurements. The fact that these galaxies were selected on the basis of their rest-frame-UV emission characteristics does argue, however, for moderate total attenuations.

The saturation of color excesses occurs for higher column densities of dust when wavelengths longer than the V-band are involved. In Fig. 5, this is illustrated in the case of a $E(V - K)$ versus $E(B - V)$ color-color plot. Here, models with increasing optical depths are plotted as series

TABLE 2
DUSTY GALACTIC ENVIRONMENT

λ	τ	τ_{att}	f(sca)	f(dir)	f(esc)	τ_{att}	f(sca)	f(dir)	f(esc)
dusty,MW			$\tau_V = 0.25$, homogeneous			$\tau_V = 0.25$, clumpy			
1000	1.309	0.589	1.07E-01	4.48E-01	5.55E-01	0.517	8.84E-02	5.08E-01	5.96E-01
1142	0.979	0.402	1.37E-01	5.32E-01	6.69E-01	0.366	1.16E-01	5.77E-01	6.93E-01
1285	0.795	0.295	1.54E-01	5.90E-01	7.45E-01	0.274	1.34E-01	6.26E-01	7.60E-01
1428	0.695	0.238	1.62E-01	6.26E-01	7.88E-01	0.225	1.42E-01	6.56E-01	7.99E-01
1571	0.646	0.215	1.61E-01	6.45E-01	8.06E-01	0.204	1.43E-01	6.72E-01	8.15E-01
1714	0.627	0.212	1.56E-01	6.53E-01	8.09E-01	0.201	1.39E-01	6.78E-01	8.17E-01
1857	0.640	0.230	1.47E-01	6.48E-01	7.94E-01	0.218	1.30E-01	6.74E-01	8.04E-01
2000	0.711	0.289	1.29E-01	6.20E-01	7.49E-01	0.270	1.13E-01	6.51E-01	7.64E-01
2142	0.798	0.353	1.13E-01	5.90E-01	7.03E-01	0.325	9.76E-02	6.25E-01	7.23E-01
2285	0.728	0.315	1.15E-01	6.14E-01	7.30E-01	0.293	1.00E-01	6.46E-01	7.46E-01
2428	0.618	0.251	1.22E-01	6.56E-01	7.78E-01	0.236	1.08E-01	6.82E-01	7.90E-01
2571	0.549	0.211	1.24E-01	6.86E-01	8.10E-01	0.200	1.11E-01	7.07E-01	8.18E-01
2714	0.506	0.190	1.23E-01	7.04E-01	8.27E-01	0.181	1.11E-01	7.24E-01	8.35E-01
2857	0.476	0.175	1.22E-01	7.17E-01	8.39E-01	0.167	1.10E-01	7.36E-01	8.46E-01
3000	0.454	0.165	1.20E-01	7.28E-01	8.48E-01	0.158	1.09E-01	7.45E-01	8.54E-01
3776	0.382	0.141	1.05E-01	7.63E-01	8.68E-01	0.136	9.61E-02	7.77E-01	8.73E-01
4754	0.300	0.111	8.85E-02	8.07E-01	8.95E-01	0.107	8.24E-02	8.16E-01	8.99E-01
5985	0.227	0.086	6.94E-02	8.48E-01	9.18E-01	0.084	6.56E-02	8.54E-01	9.20E-01
7535	0.167	0.065	5.24E-02	8.85E-01	9.37E-01	0.063	5.00E-02	8.89E-01	9.39E-01
9487	0.110	0.041	3.77E-02	9.22E-01	9.60E-01	0.040	3.65E-02	9.24E-01	9.60E-01
11943	0.076	0.030	2.53E-02	9.45E-01	9.70E-01	0.029	2.47E-02	9.46E-01	9.71E-01
15036	0.052	0.021	1.72E-02	9.62E-01	9.79E-01	0.021	1.69E-02	9.62E-01	9.79E-01
18929	0.036	0.015	1.18E-02	9.73E-01	9.85E-01	0.015	1.16E-02	9.74E-01	9.86E-01
23830	0.025	0.011	7.80E-03	9.82E-01	9.89E-01	0.011	7.68E-03	9.82E-01	9.89E-01
30001	0.017	0.008	5.11E-03	9.87E-01	9.92E-01	0.008	5.03E-03	9.87E-01	9.92E-01
dusty,SMC			$\tau_V = 0.25$, homogeneous			$\tau_V = 0.25$, clumpy			
1000	2.419	0.887	1.29E-01	2.83E-01	4.12E-01	0.733	1.04E-01	3.76E-01	4.80E-01
1142	1.860	0.671	1.62E-01	3.50E-01	5.11E-01	0.578	1.32E-01	4.29E-01	5.61E-01
1285	1.517	0.543	1.75E-01	4.06E-01	5.81E-01	0.481	1.45E-01	4.74E-01	6.18E-01
1428	1.292	0.455	1.83E-01	4.51E-01	6.35E-01	0.409	1.53E-01	5.11E-01	6.64E-01
1571	1.134	0.393	1.85E-01	4.89E-01	6.75E-01	0.359	1.57E-01	5.42E-01	6.98E-01
1714	1.018	0.345	1.87E-01	5.21E-01	7.08E-01	0.318	1.60E-01	5.68E-01	7.28E-01
1857	0.925	0.313	1.83E-01	5.48E-01	7.32E-01	0.290	1.58E-01	5.91E-01	7.49E-01
2000	0.845	0.287	1.77E-01	5.74E-01	7.50E-01	0.268	1.53E-01	6.11E-01	7.65E-01
2142	0.775	0.267	1.68E-01	5.97E-01	7.65E-01	0.250	1.47E-01	6.32E-01	7.79E-01
2285	0.714	0.249	1.61E-01	6.19E-01	7.80E-01	0.234	1.41E-01	6.50E-01	7.91E-01
2428	0.660	0.232	1.53E-01	6.40E-01	7.93E-01	0.219	1.36E-01	6.68E-01	8.03E-01
2571	0.613	0.218	1.46E-01	6.58E-01	8.04E-01	0.206	1.29E-01	6.84E-01	8.14E-01
2714	0.571	0.206	1.38E-01	6.76E-01	8.14E-01	0.196	1.23E-01	6.99E-01	8.22E-01
2857	0.533	0.190	1.35E-01	6.92E-01	8.27E-01	0.181	1.21E-01	7.13E-01	8.35E-01
3000	0.508	0.181	1.31E-01	7.03E-01	8.35E-01	0.173	1.19E-01	7.23E-01	8.41E-01
3776	0.403	0.149	1.09E-01	7.53E-01	8.62E-01	0.143	9.93E-02	7.68E-01	8.67E-01
4754	0.305	0.115	8.82E-02	8.04E-01	8.92E-01	0.111	8.19E-02	8.13E-01	8.95E-01
5985	0.220	0.084	6.73E-02	8.52E-01	9.20E-01	0.081	6.36E-02	8.58E-01	9.22E-01
7535	0.157	0.061	5.02E-02	8.91E-01	9.41E-01	0.059	4.81E-02	8.94E-01	9.42E-01
9487	0.108	0.041	3.64E-02	9.24E-01	9.60E-01	0.040	3.53E-02	9.26E-01	9.61E-01
11943	0.068	0.027	2.29E-02	9.51E-01	9.74E-01	0.026	2.24E-02	9.52E-01	9.74E-01
15036	0.041	0.017	1.40E-02	9.69E-01	9.83E-01	0.016	1.37E-02	9.70E-01	9.84E-01
18929	0.028	0.012	8.95E-03	9.80E-01	9.89E-01	0.012	8.79E-03	9.80E-01	9.89E-01
23830	0.019	0.008	5.78E-03	9.86E-01	9.92E-01	0.008	5.70E-03	9.86E-01	9.92E-01
30001	0.008	0.003	2.47E-03	9.94E-01	9.97E-01	0.003	2.43E-03	9.94E-01	9.97E-01

of connected symbols, starting with $\tau_V = 0$ at the origin. The separation of symbols from one another along a given reddening line is a measure of how each color excess scales with optical depth. Not only is the reddening line not a simple *arrow* (with the exception of the homogeneous SHELL model), the detailed shape of the reddening line depends on the dust/star geometry and the structure of the dusty medium. Of particular interest again is the clumpy SHELL geometry, which shows the initial saturation in $E(B - V)$ when clumps become optically thick in the V-band, followed by a saturation in $E(V - K)$ at much higher radial dust column density when the same clumps reach the optically thick state in the K-band. Finally, after clumps are sufficiently thick to block light in all bands, the interclump medium begins to dominate the reddening process. Where and when this occurs depends on the ratio of densities in the clump and the interclump medium. In a real physical system where the differences between different phases are rather more gradual than the fixed ratio assumed in our models, the transition shown in Fig. 5 between the reddening caused by the clumps and that caused by the interclump medium will also occur in a less abrupt manner.

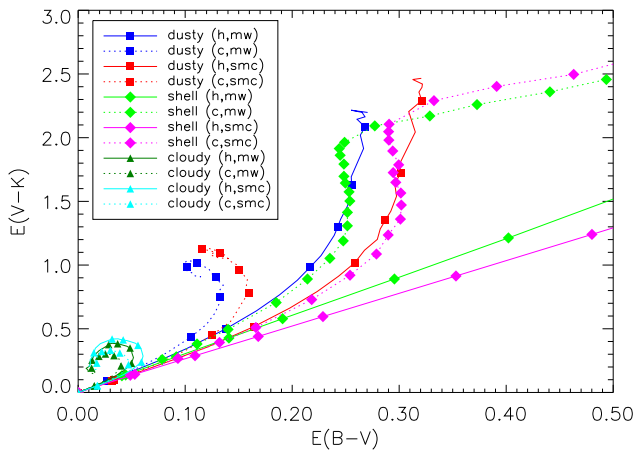


FIG. 5.— $E(V - K)$ is plotted versus $E(B - V)$. The location of the symbols along each line indicated the change in colors as the optical depth is increased. For the SHELL geometry, the symbols are plotted for every model τ_V point. For the DUSTY and CLOUDY, the symbols are plotted for every fourth model τ_V point.

3.3. Attenuation Functions

In Fig. 6, we present the predicted attenuation optical depths (see equation 1) as a function of inverse wavelength for MW dust for three cases, the optically thin case for $\tau_V = 0.5$ (top), the moderately optically thick case $\tau_V = 1.5$ (middle), and the very optically thick case $\tau_V = 4.5$ (bottom). Also shown in each panel is the average galactic extinction for the same dust column densities. While the left-hand panels show the absolute values of the respective optical depths, the corresponding right-hand panels present the same data normalized at V, in order to facilitate the comparisons of the changes in the wavelength dependence of each function. The DUSTY, SHELL, and CLOUDY models are contrasted in both their homogeneous and their clumpy forms. Fig. 7 presents the

analogous set of data for SMC dust. Insert boxes are included to show the behavior of those curves which go out of bounds vertically on the main graphs.

Several significant conclusions can be drawn from the illustrated cases. In all instances, attenuation optical depths for the three geometries are less than the interstellar extinction produced by the same column density of dust. This difference is due to the return of scattered radiation in all cases, exclusively so in the case of the SHELL geometry, and also due to lower attenuation in cases of stars only lightly embedded in the dust distribution, which is happening in the CLOUDY and DUSTY geometries. The descending order from SHELL, to DUSTY, to CLOUDY geometry can thus be understood. Similarly, clumpy structures containing the same amounts of dust as corresponding homogeneous structures always provide less attenuation than the homogeneous ones at all wavelengths. More importantly, and this difference is particularly prominent in the SHELL geometry, the clumpy structures provide a substantially grayer wavelength dependence for the attenuation than would have been expected from adopting the original extinction curve. The trend toward gray attenuation increases strongly with increasing column density, because an increasing fraction of the total attenuation is caused by clumps which are optically thick shortward of the V-band. For this same reason, the relative strength of the 2175 Å UV extinction feature, prominent in the MW dust, is greatly reduced in clumpy structures. This is in contrast to the case of the homogeneous SHELL model, which exhibits a 2175 Å feature even stronger than that in the interstellar extinction (Fig. 6, RHS). This is due to the fact that the albedo of MW dust displays a minimum coinciding with this feature, leading to return less scattered light here than at wavelengths immediately longward or shortward of the feature. Similarly, the declining dust albedo shortward of 1500 Å causes the predicted attenuation curve for the homogeneous SHELL model curves to be steeper in the far UV than the interstellar extinction curve.

It is important to recognize that the slope of the attenuation functions in the UV for the more realistic embedded and clumpy geometries is dependent on the total dust column density. The use of a single attenuation function, for example the widely used “Calzetti Attenuation Law” (Calzetti 1997), for the dereddening and flux correction of individual starburst galaxies is therefore not justified in the absence of information about the dust column density. A comparison of the “Calzetti Attenuation Law” with predictions from our models will be discussed in more detail in Section 4.

3.4. Scattered Light Component

The integrated light of dusty galaxies consists of a certain fraction of scattered light, with a spectrum similar to that of the integrated star light. This fraction depends on wavelength, geometry, total dust column density, and dust scattering properties, as well as viewing direction in the case of disk galaxies. In the latter, the relative fraction of scattered light is largest in directions perpendicular to the disk, this being the direction in which the escape probability is highest for both stellar and particularly for scattered radiation. Given the spherical geometry of our models, we are able to predict the direction-averaged scattered light

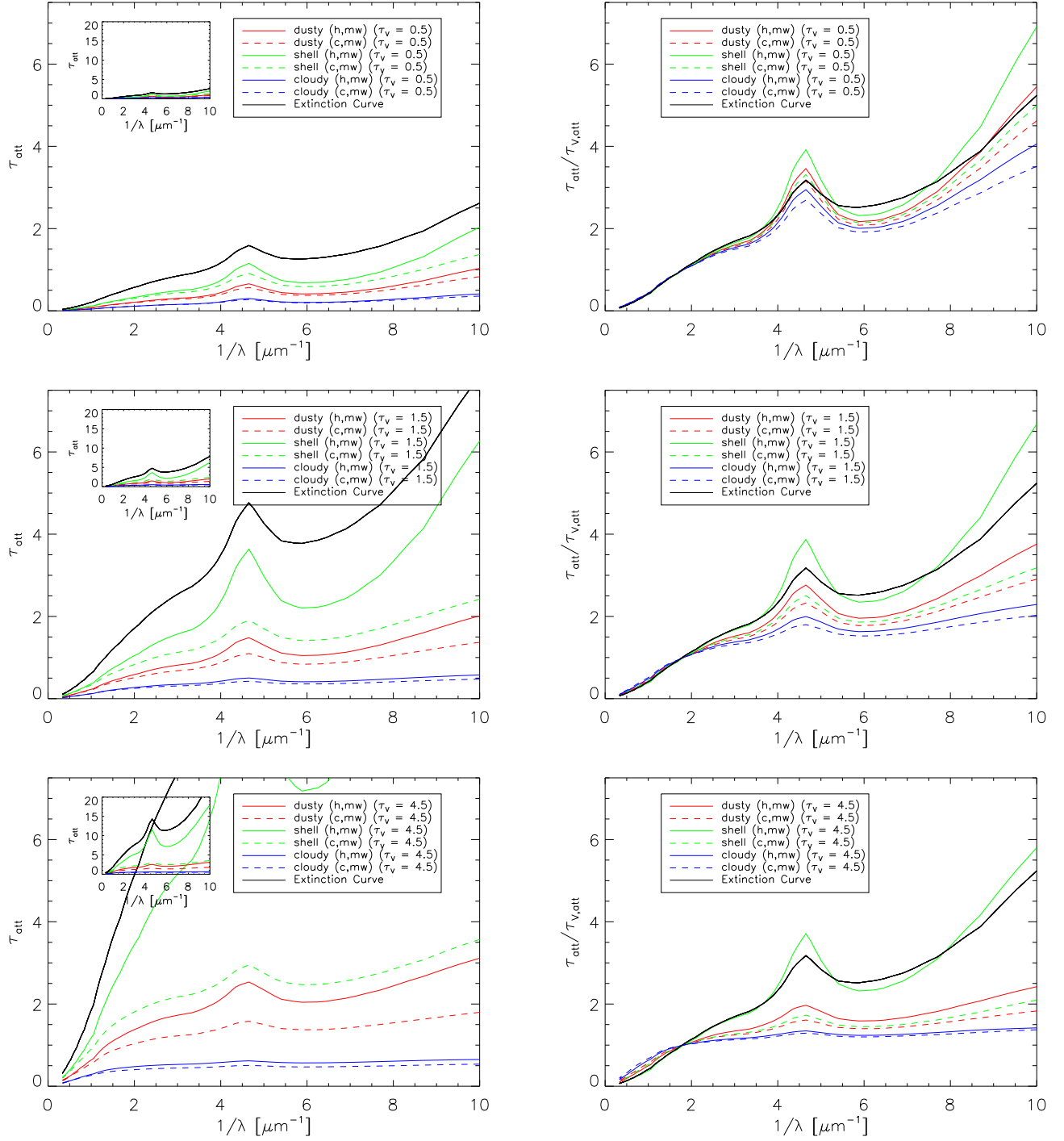


FIG. 6.— The attenuation curves for the Milky Way model runs are plotted unnormalized (left) and normalized (right).

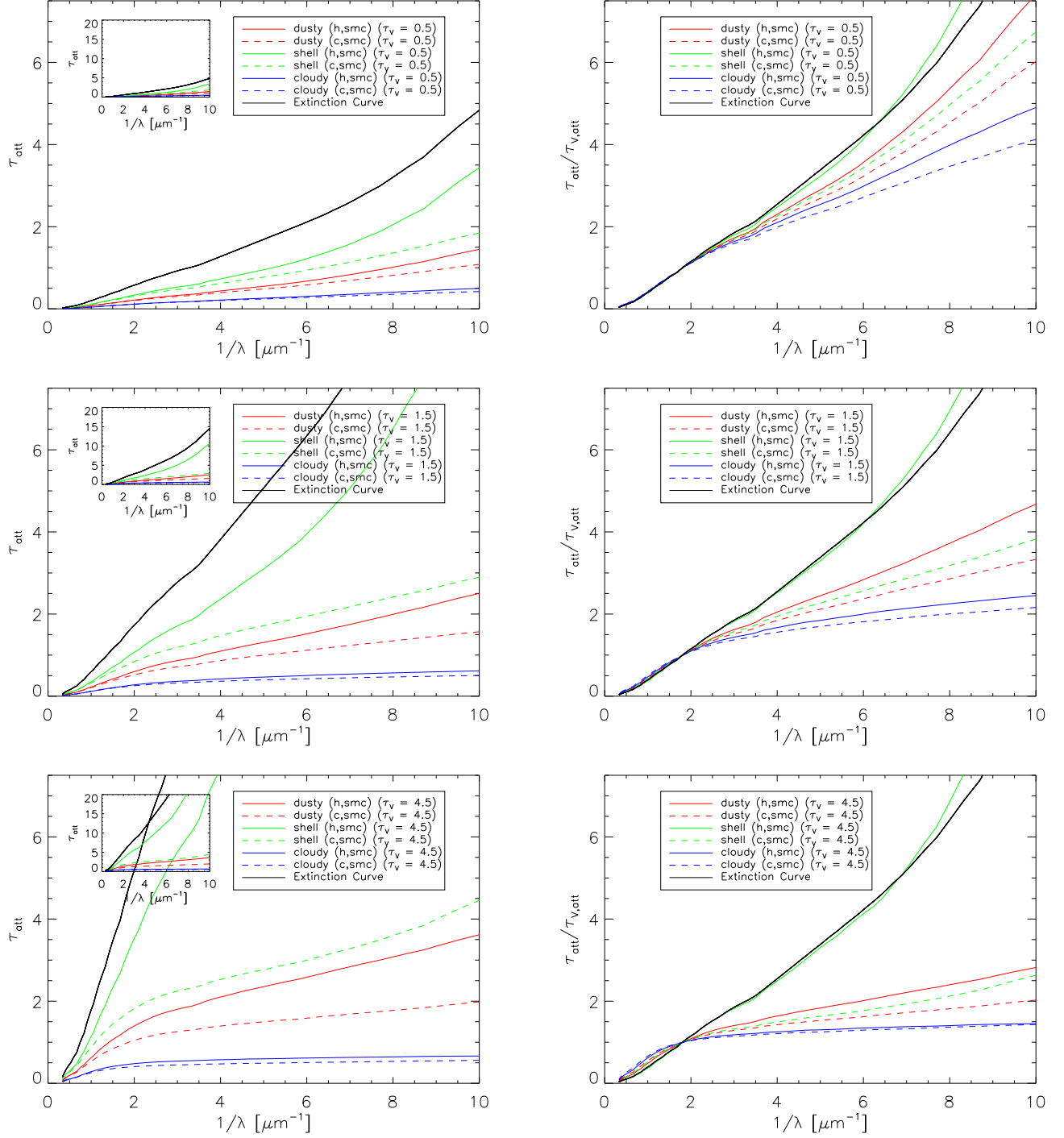


FIG. 7.— The attenuation curves for the Small Magellanic Cloud model runs are plotted unnormalized (left) and normalized (right).

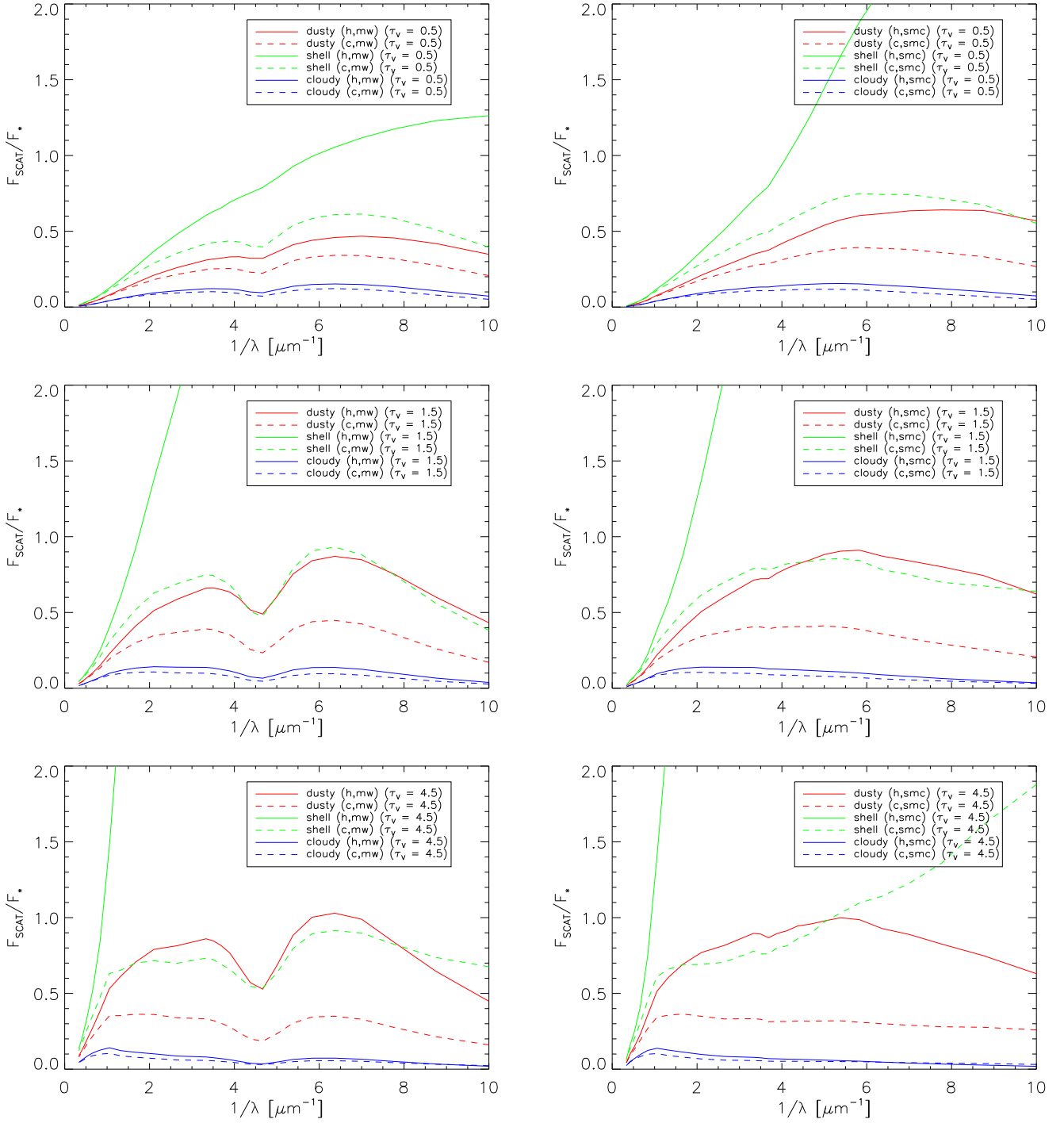


FIG. 8.— The ratio of scattered to stellar flux (F_{SCAT}/F_*) are plotted for the Milky Way (left) and SMC (right) model runs.

components. These are shown in Fig. 8 as fractions of the attenuated stellar flux for three characteristic visual radial optical depths (0.5, 1.5, 4.5), and for three geometries with both MW and SMC dust, both clumpy and homogeneous.

As expected from observations of reflection nebulae with embedded stars (Witt et al. 1992a, 1993), the scattered light fraction for homogeneous SHELL models easily exceeds unity and rises strongly with increasing optical depth, more as a result of the increasing attenuation of the starlight, less as a result of increasing scattered light flux. We view the embedded DUSTY, the clumpy SHELL models, and the CLOUDY models to be representative of actual geometries of galaxies. For these, the scattered light fraction appears to be fairly constant across the UV/visible spectrum and is likely between a quarter and one half of the total integrated light. In the case of the MW dust, the depression near $4.6 \mu\text{m}^{-1}$ is due to the albedo minimum associated with the 2175 \AA extinction bump, and this feature is actually seen in the spectrum of the diffuse (i.e. scattered) galactic light (Witt & Lillie 1973). The transition from homogeneous to clumpy structures is associated with a substantial reduction of the fractional scattered light flux. This is due to two causes: Direct starlight escapes more easily from the system, mainly through gaps in the clump distribution, while the scattered light flux is diminished, because clumps are mainly illuminated externally with the scattered light being directed preferentially into the clump interior where final absorption is more likely. In clumpy media, clumps in effect become the scattering centers instead of individual dust grains. As shown in WG96, the effective albedo of clumps is always lower than the input dust albedo. Overall, the fractional amounts of scattered light for MW dust and for SMC dust are about the same for identical dust column densities.

3.5. Variation in Clumpiness Parameters

We have emphasized that the models involving clumpy dust distributions presented in the paper are based upon one particular set of clumpiness parameters ($ff = 0.15$, $k_2/k_1 = 0.01$, $N = 30$). This set was found by WG96 to be closest to that representing the structured ISM in the Galaxy. Detailed results on how the radiative transfer is affected when the clumpiness parameters are varied can be found in WG96 as well. Here we summarize the principal effects.

The density ratio k_2/k_1 and the filling factor ff together control the contributions to the total opacity made by the interclump medium and the clumps. Our case of $ff = 0.15$ and $k_2/k_1 = 0.01$ is intermediate to the case of k_2/k_1 near unity, where the interclump medium controls the system opacity, with results very similar to the homogeneous case ($k_2/k_1 = 1.0$) and the case of $k_2/k_1 < 10^{-3}$, where the opacity is controlled by the blocking effect of the clumps and is then proportional to the filling factor. As the filling factor increases, the appearance of the system will approach that of the homogeneous case.

The grayness of the attenuation (Section 3.3) increases as k_2/k_1 decreases for the same amount of dust. Also, the ratio of scattered light to direct, partially attenuated stellar light (Fig. 8) decreases as the ratio k_2/k_1 decreases, both as a result of the growing probability of stellar light escaping without any interaction and as a consequence of the lower scattering ability of a medium dominated by

increasingly optically thick clumps. Finally, for a given amount of dust, the overall opacity of the medium will increase as the number of clumps (N) increases.

4. DISCUSSION

In this section we discuss which of our models with respect to geometry, optical depth, and dust type might best be used for the analysis of observations of different kinds of galaxies. In particular, we concentrate on dust attenuation studies of nearby starburst galaxies and Lyman break galaxies.

4.1. The “Calzetti Attenuation Law”

Starburst galaxies exhibit a wide range of dustiness as evidenced by large variations in the UV spectral index β , ratios of recombination line strengths, and ratios of far-IR to UV luminosities. The UV spectral index β was defined by Calzetti et al. (1994) through the relation $F(\lambda) \propto \lambda^\beta$ in the range $1250 < \lambda < 2600 \text{ \AA}$. By comparing the spectral energy distributions (SED) of more highly reddened starbursts with those of barely reddened starbursts, Calzetti et al. (1994) derived the observed wavelength dependence of the dust attenuation in these systems. The attenuation function takes into account the return of scattered light into the integrated light of a galaxy and also reflects radiative transfer effects arising in the three-dimensional distributions of stars, gas, and dust in these galaxies. This observed attenuation function, further refined in Calzetti (1997), is referred to in the literature as the “Calzetti Attenuation Law” or “Calzetti Law”. This attenuation due to internal dust must be clearly distinguished from the wavelength dependence of interstellar extinction, which is the attenuation due to absorption *and* scattering by a screen of dust located between a distant source and an observer.

The principal characteristic of the “Calzetti Law” is the absence of a 2175 \AA feature. Gordon et al. (1997) showed that the “Calzetti Law” can be reproduced, if the radiative transfer in starburst galaxies is occurring in a medium with intrinsic dust properties closely resembling that of SMC dust. Also, the large range of observed reddenings, as measured by variations in the spectral index β , appears to require efficient attenuation geometries such as provided by our SHELL or DUSTY geometries.

In Fig. 9 we compare attenuation values derived from starburst galaxies by Calzetti (1997) with our model attenuation functions. In order to facilitate this comparison, models and observations are renormalized to $E(\lambda - V)/E(B - V)$. In order to transform the values in Table 5 of Calzetti (1997), we have used the result of Calzetti (1997) that the stellar continuum suffers 40% the reddening that the gas suffers, i.e. $E(B - V)_{\text{stellar}} = 0.4E(B - V)_{\text{gas}}$. The data point capable of discriminating between different models most clearly is the one near $6 \mu\text{m}^{-1}$, derived from the far-UV slope in the reddened SEDs of starbursts. No model with MW dust matches this data point. In addition, the lack of a 2175 \AA feature in the observations compared to the prediction of a 2175 \AA feature in the models with MW dust argues strongly against the presence of MW dust in starburst galaxies. This will be discussed further in Section 4.4.

Among SMC dust models, the same point does discriminate between dust column densities and clearly favors the

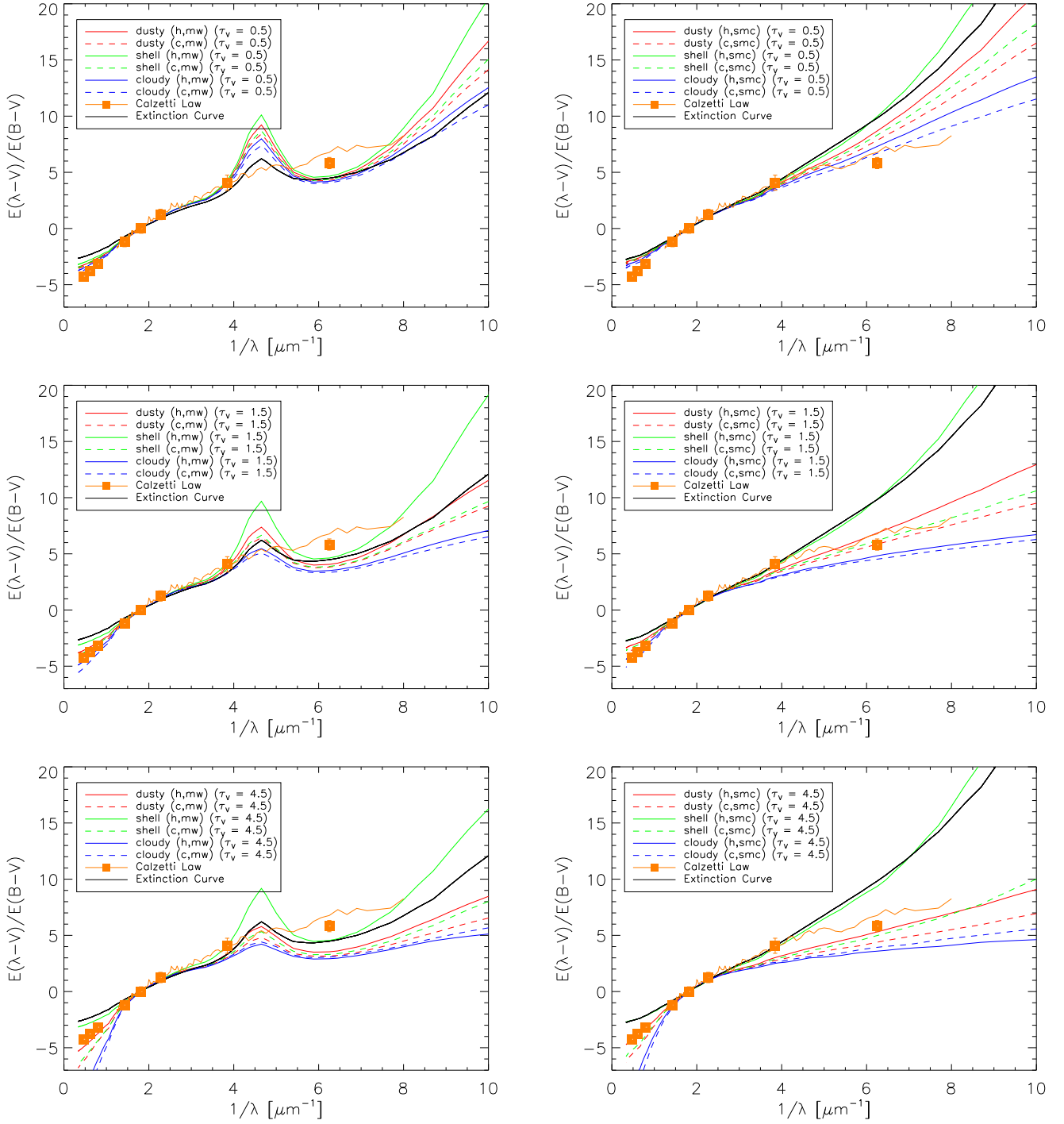


FIG. 9.— The $E(\lambda-V)/E(B-V)$ curves for MW and SMC are plotted along with the Calzetti (1997) data (filled squares) and the Calzetti et al. (1994) data (solid line) both derived from starburst galaxy observations.

clumpy SHELL model for $\tau_V = 1.5$. As is apparent from Fig. 7, such a model predicts an attenuation optical depth of about $\tau_{\text{att}} = 2.0$ at $6 \mu\text{m}^{-1}$, and, according to Fig. 4, a color excess $E(B - V) = 0.22$. An attenuation optical depth of 2.0 implies that the flux at $6 \mu\text{m}^{-1}$ has been reduced by a factor 7.4 on average in this UV-selected sample of starburst galaxies. We need to re-emphasize that there is no universal attenuation function and that the attenuation factor of 7.4 corresponds simply to the average of the sample of UV/optically-selected starbursts studied by Calzetti et al. (1994). Our average attenuation factor of 7.4 compares well with the luminosity-weighted mean absorption factor of 5.4 derived by Meurer et al. (1999) for the same sample. We discuss the UV flux reduction factor and the uncertainties associated with its determination further in Section 4.3.

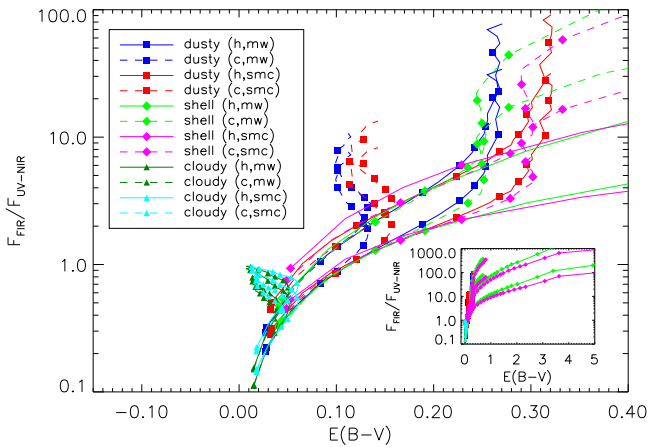


FIG. 10.— The ratio of FIR to UV-NIR flux ($F_{\text{FIR}}/F_{\text{UV-NIR}}$) is plotted versus $E(B - V)$. Each model curve is shown twice, once assuming a 1 million year old constant star formation SED and once assuming a 1 billion year old constant star formation SED. The symbols are plotted every third model τ_V point.

4.2. The Far-IR to Optical Flux Ratio

It came as an initial surprise during the IRAS mission that far-IR ultraluminous and by inference, very dust-rich, galaxies in most instances exhibited optical colors which were barely distinguishable from those of normal galaxies of similar population type. WTC showed that this was due to the fact that, given embedded dust geometries, the optical colors were determined by the least attenuated stars, while the far-IR flux was due to the absorption of light from stars which contribute little or nothing to the optical flux. The present calculations were extended to dust column densities corresponding to $\tau_V = 50$ instead of 15 in the case of WTC. In Fig. 10, we show the resulting ratios of the far-IR flux, integrated over all frequencies at which dust emission occurs, to the integrated UV/optical/near-IR stellar flux. We reproduce the most extreme observed ratios near 100 with the clumpy SHELL model of $\tau_V = 50$ with a maximum reddening near 0.8 in $E(B - V)$ and only slightly lower ratios with the homogeneous DUSTY models with a reddening less than 0.3 in $E(B - V)$. Only the homogeneous SHELL, as expected for a simple screen, produces very large amounts of reddening of $E(B - V) \sim 4.0$ and $F_{\text{IR}}/F_{\text{UV-NIR}} \sim 1000$ for $\tau_V = 50$. The fact that

most IR luminous galaxies appear to be relatively blue seems to indicate that clumpy dust structures prevail in most of them. This is also confirmed by the correlation between the ratio $F_{\text{IR}}/F_{\text{F160BW}}$ and the spectral index $\Delta\beta$ for different geometries and dust types, shown in Fig. 13.

4.3. The UV Flux Attenuation Factor

A major aim of studies of high- z starbursts (or Lyman-break galaxies) is to determine the epoch of peak star formation in the history of the Universe, if such a peak indeed exists. The outcome of such an investigation depends critically upon the corrections applied for dust attenuation in the rest-frame UV continuum spectrum of the observed galaxies, given that these systems contain substantial amounts of internal dust (Dickinson 1997; Meurer et al. 1997; Heckman 1998; Meurer, Heckman, & Calzetti 1999; Steidel et al. 1999). In addition, the upcoming NASA GALEX mission is to produce about 100,000 UV galaxy spectra in order to probe the global history of star formation, and the observed UV spectral slope is to be related uniquely to the attenuation factor by which the UV flux has been reduced by dust internal to the galaxies.

Our Figures 6 and 7 already indicated some of the problems to be expected in such an approach. The attenuation functions are geometry dependent and they become increasingly gray as the dust column density increases. This means that a heavily attenuated starburst may exhibit a steep UV slope in its SED, resembling that of a barely reddened galaxy, but show a greatly reduced UV flux, corresponding to a system with little star forming activity. The chances for underestimating the star formation rate in early epochs of the Universe are therefore severe, if dust is abundant generally in the early galaxies.

Fortunately, our models provide an excellent set of tools with which to evaluate different approaches to the problem of determining the far-UV attenuation factor. In Fig. 11a we illustrate the computed attenuation factor at 1600 \AA as a function of $E(B - V)$ found for different model geometries and dust types. As anticipated above, the observation that most observed values of $E(B - V)$ for Lyman-break galaxies fall into the narrow range of 0.2 to 0.3 barely constrains the attenuation factor to the range 4 to 200. This is not very useful as a constraint. In Fig. 11b we investigate the use of the spectral index β as a tool to evaluate the attenuation factor. Our radiative transfer models do not assume a specific energy distribution for the source spectrum. Hence, we predict only the change in the spectral index β which occurs as a result of the wavelength dependent attenuation. The GALEX program advocates this particular approach by suggesting that the change in the UV slope of the galaxies' SED can be converted into information about the applicable attenuation factor. Meurer et al. (1999) have taken the additional step of calibrating the correlation between the spectral index β and the UV-attenuation, derived for nearby UV-selected starburst galaxies. In observed starburst spectra, this change in spectral index ranges from zero to 3 (Meurer et al. 1997). Our Fig. 11b reveals that correlations between the spectral index change and the UV attenuation factor are extremely model dependent and even more dependent on the type of dust present in a given system. The calibration proposed by Meurer et al. (1999) is shown in Fig. 11b as a solid black line. For this to be valid universally, one must assume that

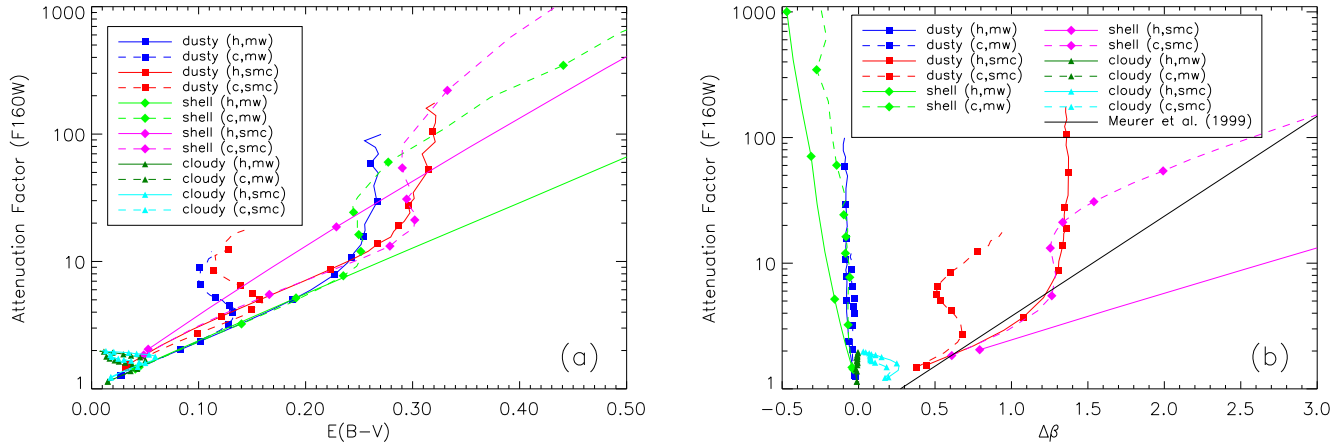
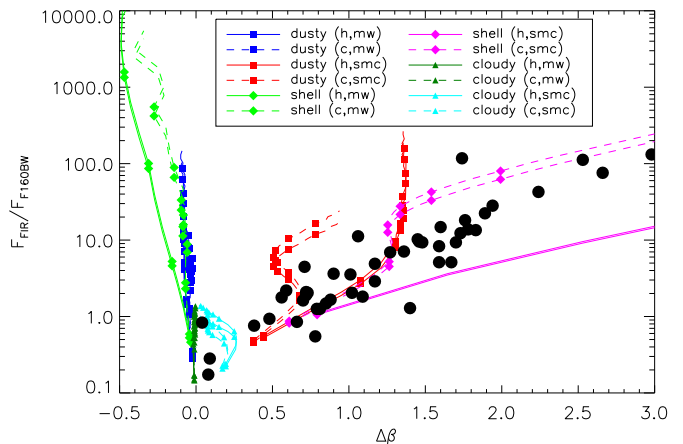


FIG. 11.— The attenuation factor in the HST/WFPC2 F160BW filter is plotted versus $E(B - V)$ (a) and $\Delta\beta$ (b). The symbols are plotted every third model τ_V point.

SMC-type dust is present in all starburst galaxies and that SHELL-type geometries with various degrees of clumpiness are the prevailing star/dust geometries. Even when restricting considerations to SMC-type dust, the range of observed values of $\Delta\beta$ is consistent with attenuation factors in the range 0–150. As is evident from Fig. 11b, MW-type dust is not expected to produce positive values of $\Delta\beta$. This is contrary to observations in starbursts, where such positive changes in the UV spectral index are seen (Meurer et al. 1999). However, MW-type dust will reveal its presence by the appearance of a 2175 Å feature. This has been seen in the heavily obscured starburst nucleus of M33 (Gordon et al. 1999a), which indicates that SMC-type dust is not a universal characteristic of all starburst environments. However, the preference for SMC-type dust in starburst galaxies is affirmed, when we compare values of $F_{\text{FIR}}/F_{\text{F160BW}}$ flux ratios and corresponding values of $\Delta\beta$ from observations (Meurer et al. 1997) with our models in Fig. 13. For this calculation we assumed that the unattenuated source SED was given by a 1 or a 1000 Myr constant star formation SED of Fioc & Rocca-Volmerange (1999). The observed data points clearly follow the trend set by the model for clumpy SHELL configurations with SMC dust. This agreement would become even more convincing, were we to present models with different ratios of clump to interclump density, different clump size, and different filling factors, which is, however, beyond the scope of this present discussion. The demonstrated model dependence of the ratio of FIR to F160BW flux suggests that the observed scatter in the data points is most likely real, as was concluded by Meurer et al. (1999) also. The spread in the FIR to F160BW ratio for a given value of $\Delta\beta$ corresponds to a factor of 10 uncertainty in the corresponding UV attenuation factor. We conclude, therefore, that the UV spectral slope is not a reliable indicator of the dust attenuation in a given galaxy. It is usable only, if a large sample of starburst galaxies with relatively uniform characteristics is being considered at once.

In Fig. 12a, we plot the ratio of dust-emitted IR flux to the integrated UV–NIR flux against the attenuation factor at 1600 Å. The model calculations assume two starbursts of different ages, one a 1 million year old constant

star formation SED, the other a 1 billion year old constant star formation SED. We note that even this ratio does not yield a unique relation to the UV attenuation factor. In particular, clumpiness in a given dust distribution will reduce the attenuation at 1600 Å for a given value of the ratio of dust-emitted IR flux to the integrated UV–NIR flux, because clumpiness is associated with a much grayer attenuation function. This is particularly evident in SHELL-type geometries. Variations in the age of the starburst and the associated changes in the UV–NIR SED affect the ratio as well, leading to a significant model dependence of the predicted attenuation factor at 1600 Å. By contrast, if we plot the ratio of integrated FIR flux to the measured flux at 1600 Å against the attenuation factor at 1600 Å, as shown in Fig. 12b, the model and age dependence practically vanish. We conclude, therefore, that the UV attenuation factor can be evaluated reliably for individual galaxies only, if a complete spectral survey of the FIR emission of the galaxy is carried out and a flux measurement in the far-UV is obtained.



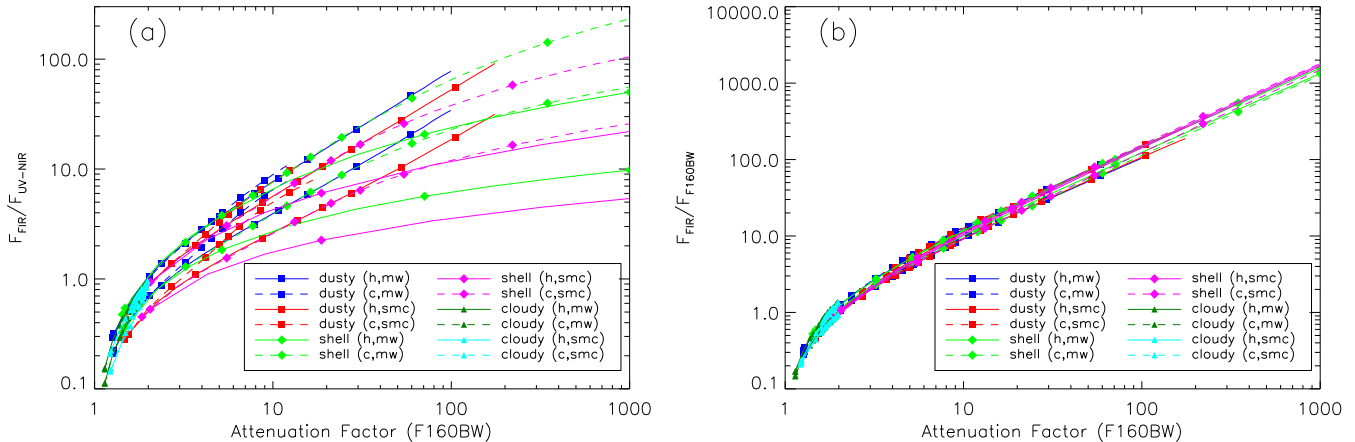


FIG. 12.— The far-IR to UV-NIR (a) and far-IR to F160W (b) flux ratios are plotted versus the attenuation factor at 1600 Å. Each model curve is shown twice, once assuming a 1 million year old constant star formation SED and once assuming a 1 billion year old constant star formation SED. The symbols are plotted every third model τ_V point.

FIG. 13.— The ratio of FIR to F160BW flux ($F_{\text{FIR}}/F_{\text{F160BW}}$) is plotted versus $\Delta\beta$. Each model curve is shown twice, once assuming a 1 million year old constant star formation SED and once assuming a 1 billion year old constant star formation SED. The symbols are plotted every third model τ_V point. The solid black points are from Meurer et al. (1999) and $F_{\text{F160BW}} \sim F_{1600} = \lambda_c f_{1600}$ and $\lambda_c = 1600$ Å. The $\Delta\beta$ values for the galaxies were computed using $\Delta\beta = \beta + 2.5$.

4.4. Lack of 2175 Å Extinction Bump in Starbursts

Gordon et al. (1997) showed that the absence of the 2175 Å extinction bump in the attenuation function of starbursts cannot be explained by radiative transfer effects but requires the actual absence of the absorber giving rise to this feature. This is despite the fact that some weakening of the 2175 Å feature was seen in the attenuation curves (Fig. 6) for embedded geometries involving MW dust and further weakening occurred when clumpiness was included. As was found by Gordon et al. (1997), the 2175 Å bump can be suppressed using radiative transfer effects, but at the expense of a gray extinction throughout the UV. Thus, the existence of a substantial slope in the Calzetti (1997) attenuation curve (Fig. 9) implies that the dust in starburst galaxies must lack the absorbers which produce the 2175 Å bump. The dust in starbursts most closely resembles that found in the SMC (Gordon & Clayton 1998). Recent modeling of this dust by Zubko (1999) shows that such dust lacks the component normally introduced to produce the 2175 Å feature (graphite), and that the overall size distribution of SMC grains is shifted toward smaller sizes compared to MW dust.

We find the color index ($F170W - F218W$) to be particularly sensitive for distinguishing between the presence of SMC dust and MW dust, one without the 2175 Å feature and the other with. In Fig. 14, we show a color-color diagram of starburst data, which are compared to the colors of unreddened starburst models (open symbols) and to reddening lines produced by our models. These reddening lines are attached to different unreddened models to show them distinctly; they may be shifted horizontally to fit the data. Several facts emerge clearly: All starburst data appear on or below the line of unreddened burst models, i.e. they are reddened in the ($F170W - F218W$) index. Only

the reddening lines for SMC dust fall below the unreddened bursts, while all MW models fall above the unreddened bursts, where no data points are found. Both the amount of reddening in the ($F170W - F218W$) index and the distribution of data points in the color plane can best be fitted with a clumpy SHELL model with SMC dust. We take this (as did Gordon et al. 1997) to be one of the strongest indications that nearby starbursts contain SMC type dust and that the prevailing geometry is that of a clumpy SHELL model. This sensitive test might be applied to the rest-frame UV SEDs of high-redshift galaxies in general in order to test for the presence of the type dust (MW or SMC).

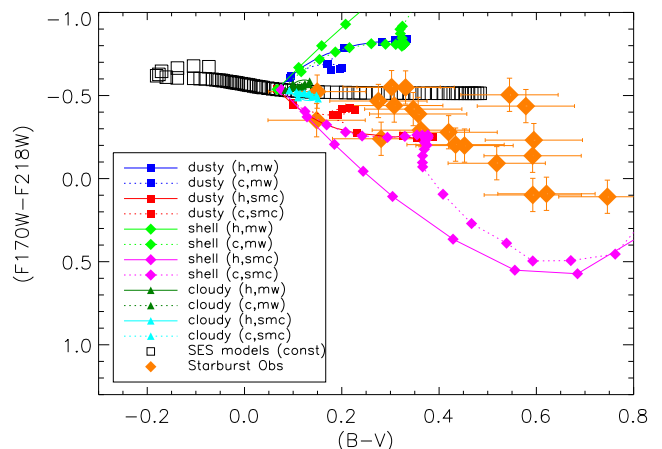


FIG. 14.— The ($F170W - F218W$) and ($B - V$) colors for starburst observations and constant star formation SES models are plotted versus each other along with the reddening trajectories predicted from our radiative transfer model. Each reddening trajectory could be attached to any of the SES model points. For this figure, we have arbitrarily attached placed the reddening trajectories to define the envelope of the starburst observations. The starburst observations all lie above [$(F170W - F218W) > -0.6$] the SES models, which is only possible if the dust in starburst galaxies is similar to that found in the SMC.

We have presented new multiple-scattering radiative transfer calculations for three representative types of galactic environments and two dust types, as found within the Local Group in the form of the average MW and SMC type dust. Both homogeneous and two-phase clumpy dust distributions have been explored over a large range of dust column densities, measured by $\tau_V = 0 - 50$. The full numerical details of the models are made available to the community via the authors, the authors WWW site, and eventually various national/international data centers. The environments examined include DUSTY, a fully mixed spherical distribution of dust and embedded stars; SHELL, a dust-free star filled region, surrounded by a dust shell; and CLOUDY, a mixed dust-star region surrounded by stars in a dust-free region on the outside. The models cover the wavelength range 1000 Å to 30000 Å with exceptionally close coverage of the rest-frame UV. This aspect makes these models particularly applicable to UV-selected starburst galaxies and Lyman-break galaxies.

We examined the models with respect to predicted reddening effects, attenuation functions, and the contribution of scattered light to the total flux as a function of wavelength. All model types except the homogeneous SHELL model exhibit reddening saturation effects. In particular, models that are likely representatives for starburst galaxies show values of $E(B - V)$ not in excess of 0.3, despite a large range of dust column density. Reddening “vectors” in color-color diagrams are complex non-linear functions depending on the prevailing dust type and structure, as well as on the geometry. Attenuation functions, which measure the wavelength-dependent reduction in the total stellar and scattered flux from a dusty galaxy, exhibit a trend toward increasing grayness with increasing dust column density. This trend is stronger in clumpy dust distributions than in homogeneous ones. No justification

was found for the use of a universal attenuation function for the analysis of a large sample of galaxies. In particular, we found that the widely-employed “Calzetti Law” is most closely reproduced by our clumpy SHELL model with SMC-type dust and a dust column density corresponding to $\tau_V = 1.5$. Such a case corresponds to an attenuation optical depth in the UV of $\tau_{\text{att}} = 2.0$ or a UV attenuation correction factor of 7.4. The Calzetti law is valid for statistical samples which have similar dust/star geometries as found in UV-selected starbursts and which have dust column densities within narrow limits. Under no circumstances should it be used for the attenuation correction for single galaxies.

When investigating various approaches to determining this attenuation factor in general, we found that the use of the color excess $E(B - V)$ and the UV spectral index β lead to results that depend strongly on dust type, dust distribution, and source-dust geometry. Only the measurement of the $F_{\text{FIR}}/F_{\text{F160BW}}$ flux ratio promises reasonable certainty for the determination of the UV attenuation correction factor in individual galaxies. This reaffirms the need for observations of starburst galaxies and Lyman-break galaxies over the entire range of rest-wavelengths, particularly the FIR, in addition to the UV. We further showed that observations can clearly discriminate between the presence of MW-type dust and SMC-type dust through the use of a $(F_{170W} - F_{218W})$ vs. $(B - V)$ color-color diagram. When applied to existing data on UV-selected nearby starburst galaxies, a consistent prevalence of SMC dust is found.

We gratefully acknowledge support from NASA grants NAG 5-3367 and NAGW-3168 to The University of Toledo. Constructive conversations with Daniela Calzetti, Geoffrey Clayton, and Karl Misselt are also gratefully acknowledged.

REFERENCES

- Berlind, A. A., Quillen, A. C., Pogge, R. W., & Sellgren, K. 1997, *AJ*, 114, 107
- Bianchi, L., Clayton, G. C., Bohlin, R. C., Hutchings, J. B., & Massey, P. 1996, *ApJ*, 471, 203
- Boissé, P. 1990, *A&A*, 228, 483
- Bruzual, A. G., Magris, G., & Calvet, N. 1988, *ApJ*, 333, 673
- Byun, Y. I. Freeman, K. C., & Kylafis, N. D. 1994, *ApJ*432, 114
- Calzetti, D. 1997, *AJ*, 113,162
- Calzetti, D., Bohlin, R. C., Gordon, K. D., Witt, A. N., Bianchi, L. 1995, *ApJ*, 446, L97
- Calzetti, D., Kinney, A. L., & Storchi-Bergmann, T. 1994, *ApJ*, 429, 582
- Cardelli, J. A., Clayton, G. C., & Mathis, J. S. 1989, *ApJ*, 345, 245 [CCM]
- Corradi, R. L. M., Beckman, J. E., & Simonneau, E. 1996, *MNRAS*, 282, 1005
- di Bartolomeo, A., Barbaro, G., & Perinotto, M. 1996, in *New Light on Galaxy Evolution*, IAU Symp. 171, ed. R. Bender and R. L. Davies, Kluwer Acad. Publ., 363
- Dickinson, M. 1997, in *The Hubble Deep Field*, STScI Symp., eds. M. Livio, S. M. Fall, & P. Madau, (in press)
- Ferrara, A., Bianchi, S., Cimatti, A., & Giovanardi, C. 1999, *ApJS*, in press (astro-ph/9903078)
- Fioc, M. & Rocca-Volmerange, B., 1999, in preparation
- Fitzpatrick, E. L. 1999, *PASP*, 111,63
- Gordon, K. D., Calzetti, D., & Witt, A. N. 1997, *ApJ*, 487, 625
- Gordon, K. D. & Clayton, G. C. 1998, *ApJ*, 500, 816
- Gordon, K. D., Witt, A. N., Carruthers, G. R., Christensen, S. A., & Dohne, B. C. 1994, *ApJ*, 432, 641
- Gordon, K. D., Hanson, M. M., Clayton, G. C., Rieke, G. H., & Misselt, K. A. 1999a, *ApJ*, 519, 165
- Gordon, K. D., Witt, A. N., & Clayton, G. C. 1999b, in preparation
- Heckman, T. M. 1998, in *The Birth of Galaxies: Xth Recontres de Blois*, ed. B. Guiderdoni, in press
- Henyey, L.G. & Greenstein, J.L. 1941, *ApJ*, 93, 70
- Hobson, M. P. & Scheuer, P. A. G. 1993, *MNRAS*, 264, 145
- Holmberg, E. 1958, *Medd. Lund. Astron. Obs. Ser. 2*, No. 6
- Holmberg, E. 1975, *Stars and Stellar Systems IX*, Univ. of Chicago Press, 123
- Hurwitz, M. 1994, *ApJ*, 433, 149
- Kim, S.-H., Martin, P. G., & Hendry, P. D. 1994, *ApJ*, 422, 164
- Kuchinski, L. E., Terndrup, D. M., Gordon, K. D., & Witt, A. N. 1998, *AJ*, 115, 1438
- Larson, R. B. & Tinsley, B. M. 1978, *ApJ*, 219, 46
- Lehtinen, K. & Mattila, K. 1996, *A&A*, 309, 570
- Lillie, C. F., & Witt A. N. 1976, *ApJ*, 208, 64
- Meurer, G. R., Heckman, T. M., Lehnert, M. D., Leitherer, C., & Lowenthal, J. 1997, *AJ*, 114, 54
- Meurer, G. R., Heckman, T. M., & Calzetti, D. 1999, *ApJ*, in press (astro-ph/9903054)
- Misselt, K. A., Clayton, G. C., & Gordon, K. D. 1999, *ApJ*, 515, 128
- Morgan, D. H., Nandy, K., & Thompson G. I. 1976, *MNRAS*, 177, 531
- Natta, A. & Panagia, N. 1984, *ApJ*, 287, 228
- Sawicki, M. & Yee, H. K. C. 1998, *AJ*, 115, 1329
- Sawicki, M. J., Lin, H., & Yee, H. K. C. 1997, *AJ*, 113, 1
- Smith, D. A., Herter, T., & Haynes, M. P. 1998, *ApJ*, 494, 150
- Steidel, C. C. et al. 1999, *ApJ*, in press (astro-ph/9811399)
- Takagi, T., Arimoto, N., & Vasevicius, V. 1999, *ApJ*, in press (astro-ph/9902219)
- Toller, G. N. 1981, PhD Thesis, State Univ. of New York at Stony Brook
- Városi, F., & Dwek, E. 1999, *ApJ*, submitted
- Witt, A. N. 1977, *ApJS*, 35, 1
- Witt, A. N., Friedmann, B. C., Sasseen, T. P. 1997, *ApJ*, 481, 809
- Witt, A. N. & Gordon, K. D. 1996, *ApJ*, 463, 681 [WG96]
- Witt, A. N. & Lillie, C. F. 1973, *A&A*, 25, 397

- Witt, A. N., Lindell, R. S., Block, D. L., & Evans, R. 1994, ApJ, 427, 227
- Witt, A. N., Oliveri, M. V., & Schild, R. E. 1990, AJ, 99, 888
- Witt, A. N., Petersohn, J. K., Bohlin, R. C., O'Connell, R. W., Roberts, M. S., Smith, A. M., & Stecher, T. P. 1992a, ApJ, 395, L5
- Witt, A. N., Petersohn, J. K., Holberg, J. B., Murthy, J., Dring, A., & Henry, R. C. 1993, ApJ, 410, 714
- Witt, A. N., Thronson, H. A., & Capuano, J. M. 1992b, ApJ, 393, 611 [WTC]
- Witt, A. N., Walker, G. A. H., Bohlin, R. C., & Stecher, T. P. 1982, ApJ, 261, 492
- Wolf, S., Fischer, O., & Pfau, W. 1998, A&A, 340, 103
- Zubko, V. G. 1999, ApJ, in press